Materials Research. 2021; 24(3): e20200290
DOI: https://doi.org/10.1590/1980-5373-MR-2020-0290

Hydrothermal Synthesis and Evaluation of the Cu_2ZnSnS_4 for Photovoltaic Applications

D.L. Sánchez Pinzón[a,b*], J.A. Gómez Cuaspud[b], E. Vera López[b], M. Schmal[a]

[a]*Universidade Federal do Rio de Janeiro, Rio de Janeiro, RJ, Brasil*
[b]*Universidad Pedagógica y Tecnológica de Colombia, Instituto para la Investigación e Innovación en Ciencia y Tecnología de Materiales (INCITEMA), Tunja, Colombia*

Received: July 03, 2020; Revised: December 23, 2020; Accepted: February 23, 2021.

The research focused on the hydrothermal synthesis of a material based on a Kesterite structure of Cu_2ZnSnS_4 (CZTS). For this purpose, the component cations, in concentrations of 1.0 $molL^{-1}$, were placed in a steel autoclave under different temperatures conditions (200, 220, 240, 260 and 280°C) for 32 h. After, the solids were calcined at 400°C for 2 h. UV-VIS results showed that materials had a strong tendency to absorb in the region of 600-800 nm, with band-gap around 1.54 eV. XRD and Raman confirmed a structure with tetragonal geometry, preferably oriented along the (112) facet, as well as low frequency vibrational and rotational modes typical of CZTS. TEM showed nanometric crystallites (≈41.6 *nm*). XPS showed the Cu^{2+}, Sn^{4+}, Zn^{2+} and S^{4-} species in correspondence with its main oxidation states. The electrical analysis, allowed to evaluate the behavior under load conditions, suggesting a potential use these materials for photovoltaic applications.

Keywords: *CZTS, Kesterite, Semiconductor.*

1. Introduction

One of the most important global problems that have caught the attention of scientific, political and economic media is the depletion of conventional energy sources and their impact on the environment. The excessive use of fossil fuels has dramatically increased the emissions of CO_2 and other greenhouse gases. Studies have shown that in January 2019, the levels of CO_2 have reached values of 410.83 ppm and according to recent reports, during the month of January 2020, higher levels were reached, registering concentrations up to 413.40 ppm[1,2]. These records, along with statistics that estimate an energy demand around 30 TW (1TW = 10^{12} W) for the year 2050, imply changes in the energy sector[3]. The imminent transformation of the energy market has driven the research, development and application of alternative renewable technologies, which not only are potentially applicable, profitable and efficient, but also contribute to mitigate the adverse effects derived from the overexploitation of non-renewable resources[4].

Solar photovoltaic technology could potentially satisfy the energy supply, without generating carbon emissions[5]. Several solar cells models have been successfully introduced in the market, however, the scope is limited, since the development of this technology is still in its early stages[6]. The creation of new materials and the greater diversity in processing techniques have contributed enormously towards the development of these devices, so that its participation in the energy sector has taken an important leap, going from 1.0 GW at the beginning of 2002 to an estimated 227 GW by the end of the year 2015[7,8].

Solar cells based on tellurium, selenides, tertiary and quaternary chalcogenide, among others, have had a positive impact on the development of thin-film solar cells, achieving conversion efficiencies around 20% however, the manufacturing processes do not always correspond to ideal aspects of low toxicity, abundance and affordability, limiting their availability[9,10]. Thus, new generation materials based on Cu_2ZnSnS_4 type systems (abbreviated as CZTS) have attracted growing interest. CZTS is an alternative material to CdTe and CIGS. It is composed of elements which are less toxic and more available. There are two crystalline forms for CZTS, Estanite and Kesterite, the latter having greater thermodynamic stability[11]. For photovoltaic applications, Kesterite has more useful properties. CZTS is a *p*-type quaternary semiconductor due to Cu vacancies[12]. Its direct band-gap is around 1.5 eV[13] and its concentration of charge carriers is similar to CIGS type materials, having an absorption coefficient in visible wavelengths of approximately 10^4 cm^{-1} [9-13]. The efficiency of this material was only 0.67% in 1997[14] and, in the year 2014, it reached a record efficiency of 12.6%[15]. The absorbent material was manufactured using a pure hydrazine solution, however, this method is not suitable for large-scale manufacturing processes[16]. Based on theoretical calculations of the Shockley-Queisser limit, these devices could achieve efficiencies above 28%, representing an opportunity for massive employment of solar technology[17].

This investigation aims to find out photovoltaic materials and devices, with focus on the synthesis and physical-chemical characterization of Kesterite type materials based on the Cu_2ZnSnS_4 system. For such purpose we propose a hydrothermal route, which allows the incorporation of the cationic components of the material in a stoichiometric way, without the need for steps related to subsequent sulfurization processes or the implementation of high-cost vacuum processes; varying the syntheses parameters for the obtaining pure-phase

*e-mail: *dayana.sanchez@coppe.ufrj.br*

materials, with potential applications in the development of absorbent layers for photovoltaic applications.

2. Methodology

2.1. Synthesis

The CZTS materials were prepared starting from analytical precursors of Cu, Zn, Sn and S. Copper nitrate [$Cu(NO_3)_3.3H_2O$] 1.0 M, zinc acetate [$Zn(CH_3COO)_2$] 1.0 M, anhydrous tin chloride [$SnCl_2$] and thiourea [TU] all from Merck (99.9%). The reagents were mixed in corresponding stoichiometric relation 2:1:1:4 under magnetic stirring (250 rpm), for 30 min until the formation of stable mixtures in each case. The filling of the Teflon containers of the hydrothermal reactors was done until 80% of total volume of recipient, to ensure an adequate vapor pressure along hydrothermal process in each synthesized composition. The Teflon lined autoclaves were sealed and placed in an electric convection oven for the respective thermal process; the reaction conditions for all materials were defined as shown in Table 1.

The reaction produced a brown-looking precipitates that were repeatedly washed with anhydrous ethanol to remove remaining impurities from the treatment. Subsequently, the solids were dried in an oven at 100°C for two hours and finally treated at 400°C in a tubular furnace for 2 hours under conditions of N_2 flow (15 mL min^{-1})[18]. The final solids were characterized through different analytical techniques in order to identify the best synthesis conditions previous at elaboration of solar cell.

With the use of CZTS5 solid, was possible to use 0.5 g of powdered and moldered material, which was mixed with 5 mL of DMSO (Merck 99.9%), and stirred for 20 min at room temperature. The solid was dissolved under stirring until obtaining a homogeneous solution, that will be deposited as a film, using spin coating procedure operated at 1500 rpm. This film permits to cover a commercial substrate coated with Mo of 20 x 25 mm^2, previously washed with ethanol and deionized water. The method enables the deposition of 10 layers of material at 2000 rpm for 20 s. Each cycle was dried on a hot plate at 150°C for 3 min. The final substrate configuration obtained was the Mo/CZTS5/CdS/i-ZnO/ITO. All fabrication the process was developed by chemical bath deposition (CBD) and sputtering deposition methods. The last layers of i-ZnO and ITO were deposited with an approximate thickness of 50 and 400 nm, respectively, for to minimize minimizing the effects of discontinuity of the buffer layer. The deposition of these layers was made by sputtering, using a DC-magnetron equipment, in each case with targets of 99.99% purity, to obtain the corresponding current density−voltage (J−V) plots.

2.2. Characterization

The optical properties of the CZTS materials were analyzed by visible ultraviolet spectroscopy (UV-VIS), with exploration interval of 190 to 1100 nm, using a Spectrophotometer 8000 PC by Mapada Instruments. The measurements were made at room temperature, using a solution composed of 0.010 g of the material dissolved in 1.0 mL of ethylene glycol with the help of an ultrasound equipment Baku-Bk 2400 operated at 35 W and 40 kHz.

The structural characterization of the materials was carried out by X-ray diffraction (XRD), in a PANALytical X'pert PRO MPD, using the Cu Kα radiation (λ = 1.54186 Å) from 20 to 90° 2θ. The results were analyzed using the X'Pert High Score program using the ICDD databases and the crystallite sizes were calculated from the most intense diffraction signals by the Debye-Scherrer equation.

The Raman spectroscopy analyses, were performed in a HR-UV 800 infinity microprobe (Jobin-Yvon), equipped with a CCD detector (-70°C) and a 10.7 mW laser. All spectra were measured between 200 and 500 cm^{-1}, projecting a continuous laser radiation of He-Ne, which generated an excitation line at 632 nm.

Morphological and surface analyses carried out by scanning and transmission electron microscopy (SEM-TEM) made use of a JEOL JSM 6490-LV equipment, accelerated with excitation energies ranging from 0.1 to 30 KeV, in which a thin beam of electrons was focused on the samples. Also, a JEOL 2100 equipment was employed, endowed with a LaB_6 thermionic cannon, an acceleration voltage of 200 kV and a CCD camera that allows to acquire high resolution images. The micrographs were processed in the Image-J software to determine the grain size diameter and the morphology of the CZTS materials.

The X-ray photoelectron spectroscopy (XPS) analyses were carried out in the surface characterization platform XPS/ISS/UPS-A Centeno SPECS. The platform, equipped with a PHOIBOS 150 2D-DLD energy analyzer and a monochromatic Al Kα X-ray emission source (FOCUS 500), was operated at 200 W. The step energy of the hemispheric analyzer was set at 100 eV for the general spectra and 60 eV for the high resolution spectra. The surface charge compensation was controlled with a flood gun (device FG 15/40-PS FG500), operated at 58 μA and 1.5 eV. The spectra were analyzed with the CasaXPS software (Casa Software Ltd) using the CasaSSI GL 15 library for the values R.S.F. For this purpose, a Shyrley type baseline was used, while the binding energy

Table 1. Synthesis parameters for CZTS materials with values of band-gap and crystallite sizes obtained from the X-ray diffraction data and transmission electron microscopy analysis.

Material	Temperature treatment (°C)	Time (h)	Eg (eV)	Crystallite size (nm)
CZTS 1	200	32	1.69	35.0
CZTS 2	220	32	1.97	38.0
CZTS 3	240	32	1.84	39.5
CZTS 4	260	32	1.90	41.0
CZTS 5	280	32	1.54	42.3

scale (BE) was corrected using as a reference the C*1s* signal at 284 eV.

The electrical response of the solids was evaluated from solid state impedance spectroscopy (EI) at room temperature, in an AUTOLAB potentiostat-galvanostat following established protocols[14]. The data collected in a cell adapted for this purpose were taken between 0.1 and 40 MHz. For this, 0.5 g pellets under a uniaxial pressure of 5.0 Mpa were prepared for each sample. Each tablet was polished to achieve thicknesses of 5.0 mm and a homogeneous surface. Each analysis was corrected using a reference cell to reduce the noise effects during all measurements.

Finally, the electrical efficiency of a solar cell made based on the most promising material, was developed through a precision microdiamond scriber MR200 OEG equipment, for precision tracing of cells using a diamond tip tool and an optical system of positioning. The obtained cell was tested in the Sun 3000 class AAA solar simulator, Abet Technology. The apparatus is equipped with standard lighting conditions AM 1.5 and 100 mW/cm^2, where the electric parameters at open circuit voltage, short circuit current, fill factor and efficiency were determined from the data provided by the simulator.

3. Results and Analysis

3.1. Visible ultraviolet spectroscopy (UV-VIS)

Table 2 shows the estimated Band-gap values for each material, using the Tauc equation. The absorption profiles of the synthesized materials are shown in the Figure 1. The results show that CZTS materials have low transmittance levels, indicating that the solids promote adequate absorption conditions mainly concentrated in the region of 2.0-1.54 eV, which evidence media values associated to an appropriate behavior in terms of UV absorption coefficients[19].

The results show a direct relationship between the synthesis temperature and the optical properties of the materials. It was observed that the energy gap decreases as the treatment temperature increases. This behavior suggests effective electronic transitions in the valence band, so that at higher temperatures a better consolidation of the Kesterite phase was achieved, decreasing the percentage of secondary phases in the CZTS materials. Khalate et al.[20], showed similar behavior and found that the optical properties of CZTS are influenced by the temperature in processes that are clearly dependent of synthesis conditions.

In effect, the synthesized materials exhibit characteristic band-gap values for each system, in which the CZTS5 material showed a remarkable result, reaching Eg values around 1.54 eV, in accordance with work of Aixiang Wei et al.[21], who synthesized CZTS materials by chemical treatment using different solvents and found band gap values varying between 1.37 and 1.60 eV. These values disagree with our results mainly along CZTS1 to CZTS4 systems that display band-gap values ranging from 1.97-1.69 eV, demonstrating that the low synthesis temperatures in first stage of reaction, deviate from the optimal values expected for band-gap performance and solar conversion processes. This fact can be related to the presence of secondary phases thermally dependent, such as Cu_2S, SnS and Cu_2SnS_3, responsible for variation in the energy gap that affect the performance of the materials under carrier transport conditions, thus the recombination processes in the grain boundaries could be affected[22,23]. However, it was clear that the defects generated by the secondary phases in the first stage of hydrothermal synthesis are maintained, even after the second stage of reaction at 400°C, which makes it possible to determine the importance of the initial synthetic process, which enables consolidation of the main crystalline phase. This relevant result demonstrates how the first stages of consolidation of crystalline materials are decisive in reducing the concentration of secondary phases, which although these can be reduced with subsequent thermal treatments, improving the crystallinity and optical properties of the materials, it need to be attenuated from the initial stages of solid formation in the present method[24,25]. It seems that the CZTS5 material display the best results, showing nearby band-gap values as required for design of photovoltaic technologies (1.50 eV)[26-29].

Table 2. Band-gap values and crystallite sizes of CZTS samples obtained by means UV and XRD measurements.

Material	Eg (eV)	Crystallite size (nm)
CZTS 1	1.69	35.0
CZTS 2	1.97	38.0
CZTS 3	1.84	39.5
CZTS 4	1.90	41.0
CZTS 5	1.54	42.3

3.2. X-ray diffraction analyses

The structural and phase analysis performed on the CZTS samples by X-ray diffraction showed that the synthesis temperature significantly affects the morphological and structural properties of the materials, this behavior confirms the obtained results by UV-VIS and are shown in Figure 2.

The analysis of the X-ray diffraction patterns of the CZTS 5 materials allowed to determine that the solids have a phase in agreement with the reference compound Cu_2ZnSnS_4 with structure type Kesterite with crystalline orientation along (220) facet. The identification of crystalline phase is according

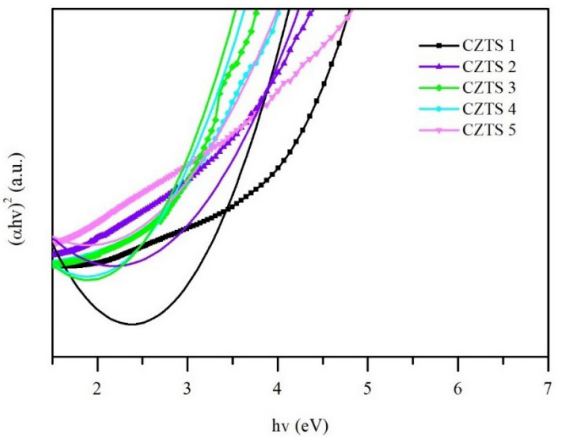

Figure 1. Plot of $(\alpha hv)^2$ vs hv for the estimation of the band gap energy of CZTS1-CZTS5.

with a tetragonal structure corresponding with the space group *I 42m* and cell parameters *a*=5.4270 Å, *b*=5.4270 Å, *c*=10.8480 Å, in relation to collection code ICSD: 00-026-0575 in accordance with previous works[18,30,31]. Although the diffractograms reveal that solids display a prevalent Kesterite phase, the Rietveld refinement carried out with the GSAS software indicate the presence of a secondary covallite phase of CuS in all cases. This phase, have a hexagonal crystalline structure with lattice parameters *a*=3.8020 Å, *b*=3.8020 Å and *c*=16.4300 Å according to the collection code ICDD: 00-001-1281. The presence of this phase in the solids is related to the synthesis temperature established in current work and becomes more evident in those materials that were synthesized at low temperatures (CZTS1-CZTS4). This relationship has been reported by Agawane et al.[32], observing that the intermediate phases of covallite, could be attributed to the incomplete transformation of sulphides at low temperatures. Moreover, non-stoichiometric relations of Zn, Sn and Cu can lead to formation of inhomogeneous materials[33].

Some works, shows that the molar ratios of [Cu]/([Zn] + [Sn]) greater than 1.0 favor the formation of secondary phases of copper sulphide (CuS), since the most conventional synthesis route is based on later sulphurization stages that use a starting material of CZT, synthesized by physical routes (due to problems related with volatilization), where the cationic radios of Cu/(Zn+Sn) and Zn/Sn ranging between 0.7–0.9 and 1.1–1.3 respectively)[34,35]. However, the current work enables the incorporation of S at chemical level, avoiding the sulphurization stage and the premature S volatilization, permitting an effective incorporation in the structure of CZTS. Such procedure, allows to evaluate the volatility of Sn with respect to other components and the subsequent understanding of how hydrothermal synthesis route affect the electrical behavior of samples, in accordance with Vishwakarma et al.[36].

Although the secondary phase of CuS, identified in all CZTS synthesized samples throughout the series, occurs at low concentrations, it is clear that it can be eliminated by the use of second reaction stages, where the material is subjected to thermal treatments between 400 and 500°C under controlled atmospheres and reaction times. In this regard, Wang et al.[37], have shown that the physicochemical properties of CZTS obtained by hydrothermal reactions can be improved, when complementary synthesis protocols are developed involving temperatures close to or equal to 500°C, thus optimizing the main phase of Kesterite[38].

Based on these results, among synthesized materials, the CZTS5 show the most important advantages from the structural point of view, with respect to the other obtained materials, indicating that the crystalline nature of CZTS5 was improved with the initial treatment at 280°C. The results shown in Table 2, using the Debye Scherer's equation for the most intense diffraction signals, are consistent with the synthesis methodology and preliminary results, being evident that the hydrothermal synthesis temperature influence the crystallite size of these materials. Thus, the obtention of solids with larger sizes is favorable, since the recombination processes of load carriers take place in grain boundaries, so that the efficiency is improved during solar conversion processes as established by Vanalakar and others[39-42].

3.3. Raman spectroscopy analyses

The Raman microscopy analyzes carried out on the CZTS solids showed that in addition to the characteristic signals of the CZTS material secondary phases of Cu_2SnS_3, Sn_2S_3, SnS_2, are observed along CZTS1-CZTS5 materials, mainly in the case of $Cu_{2-x}S$ and ZnS phases, being clear a notable evolution in terms of synthesis temperature. The consolidation of a Kesterite phase is more evident in CZTS5 sample, with a strong signal around 287 cm^{-1}, as indicated in Figure 3.

The signals of magnified Raman spectrum of CZTS5 sample is shown in Figure 4, and exhibit a more detailed evidence of secondary phases with the main peak related with the Cu_2ZnSnS_4 system in the Kesterite phase. The figure shows a signal at 338 cm^{-1} related to the A-asymmetric vibrational mode of the Kesterite. This mode linked to the vibrations of the sulfur atoms in the crystal lattice is associated with the main signal of the CZTS molecule[18,44]. Likewise, the intense signal found at 287 cm^{-1} is related to the characteristic phononic frequencies of CZTS. The signals at 243, 255 and 257 cm^{-1} are also associated with the CZTS material. These signals are similar with the results reported previously in the literature[44-46].

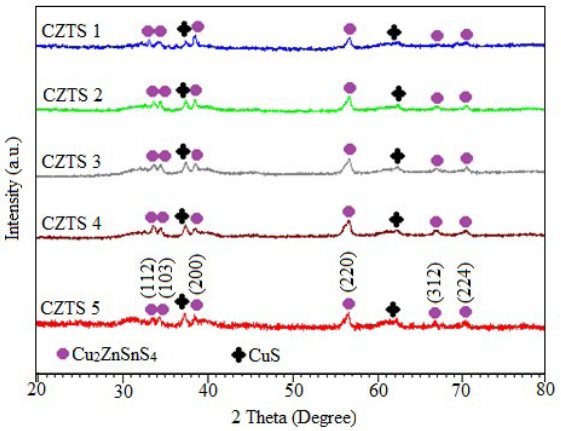

Figure 2. X-ray diffraction pattern for CZTS1-CZTS5 systems between 20 and 90° 2θ showing the formation of the Cu_2ZnSnS_4 and CuS phases.

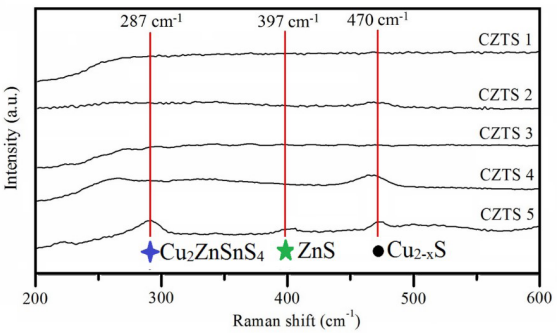

Figure 3. Evolution of main vibrational Raman signals along CZTS1-CZTS5 samples with presence of secondary phases of ZnS and Cu_2S.

In the CZTS works developed by Gürel et al.[47], and Khare et al.[48], the theoretical frequencies related to the main modes of vibration of CZTS in the Kesterite phase were calculated. Gürel estimated these signals around 325 cm^{-1} (vibrational mode A), 289 cm^{-1} (vibrational mode E (LO)) and 366 cm^{-1} (vibrational mode B (TO)), while Khare found these same signals at 338, 278-290 and 373 cm^{-1} respectively. These results, in addition to being consistent with the frequencies of displacement of the vibrational and rotational states expected for our composition, confirm the presence of the Kesterite phase in the CZTS5 material. The signals located at 224, 305, 325, 362, 368, 397, 420 and 470-476 cm^{-1} are associated with the presence of Cu_2SnS_3, CuS, Sn_2S_3, SnS_2, ZnS and $Cu_{2-x}S$ in the materials, however, these phases are expected to be integrated into the crystalline phase of Kesterite after a second heat treatment. In this sense, it demonstrates the positive effect of the higher temperatures of synthesis to obtain a more stable chemical and crystalline composition[49].

3.4. Scanning electron microscopy (SEM)

The morphological aspects and surface characteristics of the CZTS materials were analyzed by scanning electron microscopy. The results shown in Figure 5, reveal that the solids are conformed by homogeneous multiparticle aggregates of irregular spherical geometry. It was not possible to distinguish a morphological and at a superficial level the five systems, however, in accordance with the works reported by Wang et al. The morphology of these materials was improved with increasing synthesis temperature, since the concentration of agglomerates decreased noticeably[50].

Elemental composition analyzes performed on the CZTS samples, using X-ray dispersive energy spectroscopy (EDX), revealed that the experimental compositions differ about 1% with the theoretically calculated compositions (Table 3). This difference can be caused by the tendency of zinc and tin towards the formation of sulfides at low temperatures; however, based on the properties identified up to this point and by effect of the low synthesis temperatures, it is expected that these products could be reduced in posterior thermal treatments to help to consolidate the main phase of Cu_2ZnSnS_4.

The EDX spectra shown in Figure 6, demonstrate that the Kα signals are correlated with the proposed compositions and the values reported in the literature[51].

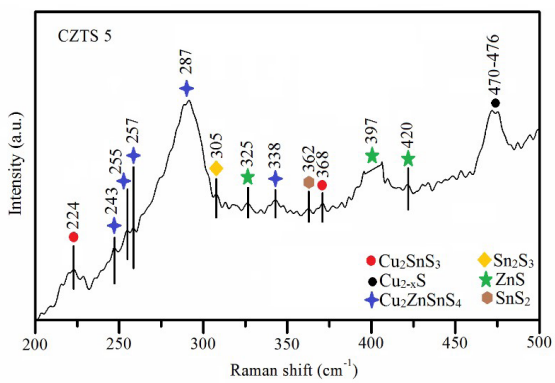

Figure 4. Raman magnified spectrum for the CZTS5 system showing the signals associated with the vibration bands[43].

3.5. X-ray diffraction analyses (CZTS 5)

Based on the preliminary results, it was possible to determine that the materials obtained at low temperature, have the highest levels of instability and higher proportion of secondary phases, being evident that its reaction conditions must be adjusted to achieve better physicochemical characteristics for possible photovoltaic applications. In this sense, we perform an additional thermal treatment of CZTS5 material at 400°C for 2 hours in a nitrogen atmosphere using a flow of 15 $mLmin^{-1}$, in order to consolidate even more the crystalline phase. The X-ray analysis confirmed a significant advance in the crystallinity of the CZTS5 material, as shown in Figure 7, where it is notable that the diffraction signals characteristic and indexed with the diffraction facets (112), (220) and (312) increased its intensity, reflecting a higher content of the Kesterite phase in the solid. Similarly, the signals found for this system are in accordance with the works developed by Shen et al.[52], and other authors[39,53,54], who report the obtaining of a similar characteristic.

3.6. Raman spectroscopy analyses (CZTS 5)

The Raman analysis of the sample after the second thermal treatment indicates that the signals associated with the secondary phases of Cu_2SnS_3, Sn_2S_3, SnS_2, $Cu_{2-x}S$ diminish significantly their intensity almost until disappearing completely, as shown in Figure 8.

The two dominant signals at 336 cm^{-1} and 256 cm^{-1}, are related to the sought phase of Kesterite. The signals located at 240 and 256 cm^{-1} also correspond to the vibrational modes of this material. The less intense signals at 309, 359 and 372 cm^{-1} are associated with a low concentration of SnS and ZnS that remain after the calcination step, in the main crystalline network. In fact, the signals agree with the frequencies reported in the literature, indicating that the additional thermal treatment was successful to minimize the formation of sulfides[47,48].

Table 3. Percentage composition of the CZTS materials obtained by X-ray dispersive energy spectroscopy (EDX).

Composition	Cu	Zn	Sn	S	Total
Theoretical composition	28.91	14.87	27.03	29.03	99.99
CZTS 1	28.93	14.73	27.04	29.30	100
CZTS 2	28.85	14.73	27.00	29.41	100
CZTS 3	28.77	14.87	27.10	29.26	100
CZTS 4	29.15	14.23	27.63	28.99	100
CZTS 5	28.65	15.69	26.89	28.77	100

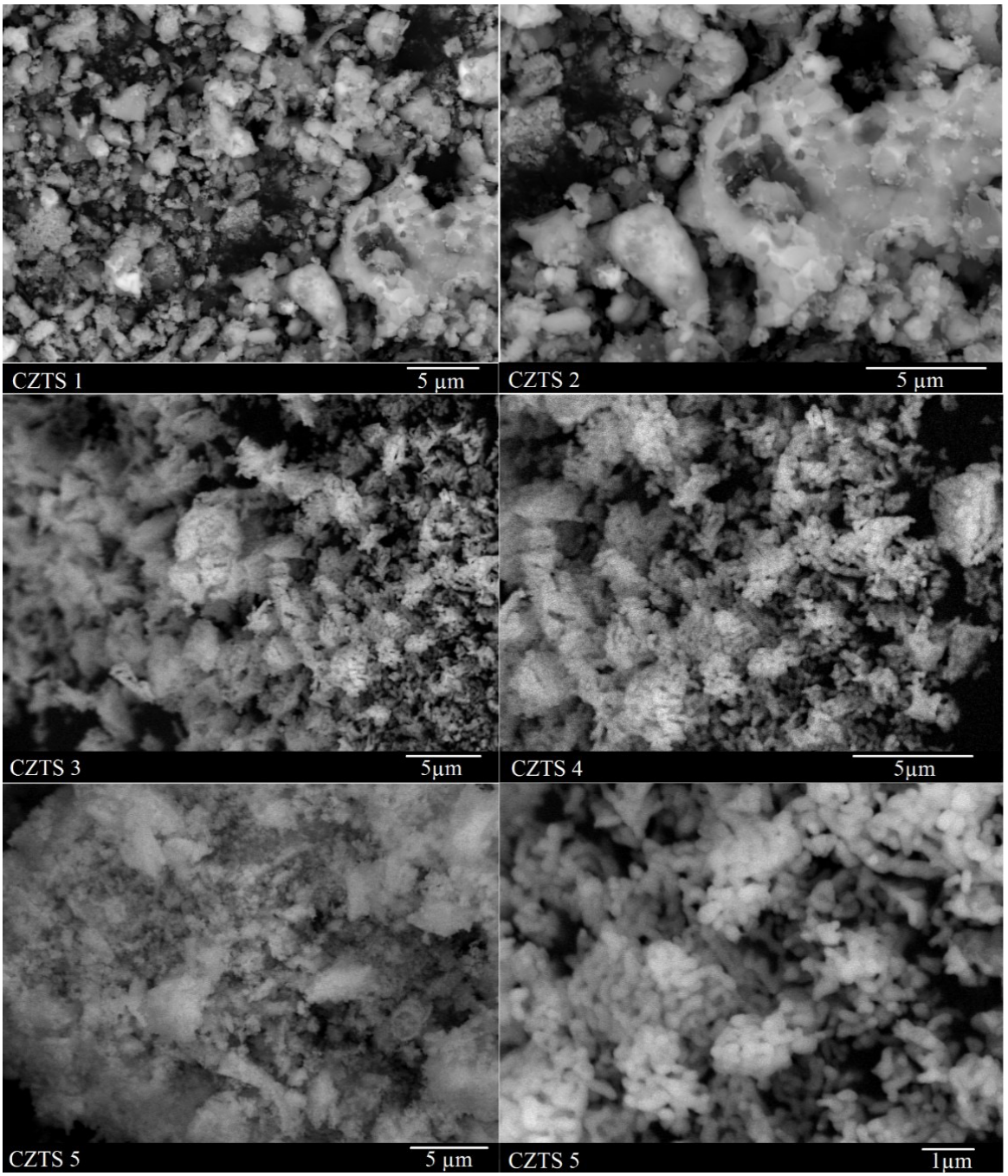

Figure 5. Scanning electron micrographs for CZTS1-CZTS5 systems. CZTS 5 material[18].

3.7. Transmission electron microscopy (TEM)

The results derived from the TEM analyses show that, despite of the thermal treatment, the CZTS5 material presents a nanometric structure conformation as shown in Figure 9.

The micrographs revealed the presence of crystallites of regular geometry and crystallite sizes between 29.7-41.6 nm. The calculated frequency histogram shows a distribution of concentrated particle sizes is around 41.6 nm.

3.8. X-ray photoelectron spectroscopy (XPS)

X-ray photoelectron spectroscopy (XPS) analysis performed on the CZTS5 sample demonstrates the presence of signals at 163 and 169 eV (Figure 10) that are compatible with the characteristic bonds for metal sulfides ($2_{p3/2}$ and $2_{p1/2}$ respectively). In this way an oxidation state 2^- is established for this element[55,56].

The signals related to $Sn3_{d5/2}$ and $Sn3_{d3/2}$ are located at 487 and 496 eV, confirming a 4^+ oxidation state. The signals

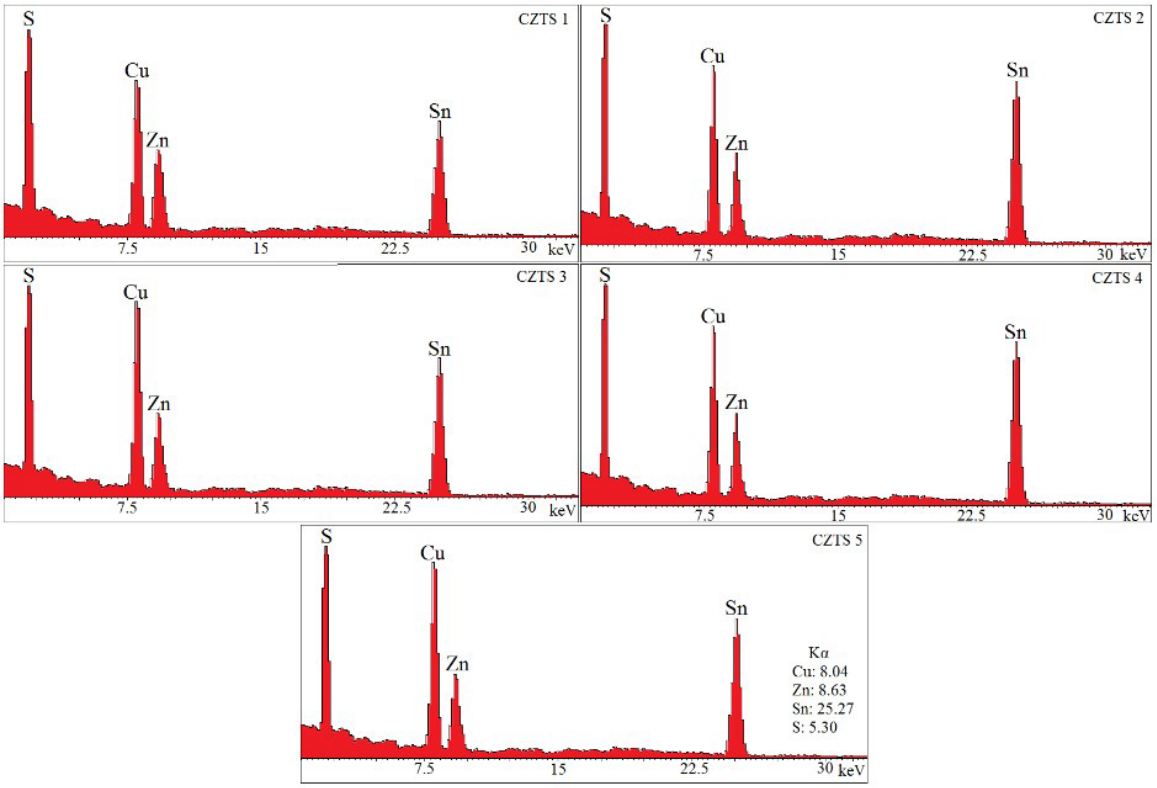

Figure 6. Microanalysis by dispersion of X-ray energy for CZTS1-CZTS5 systems.

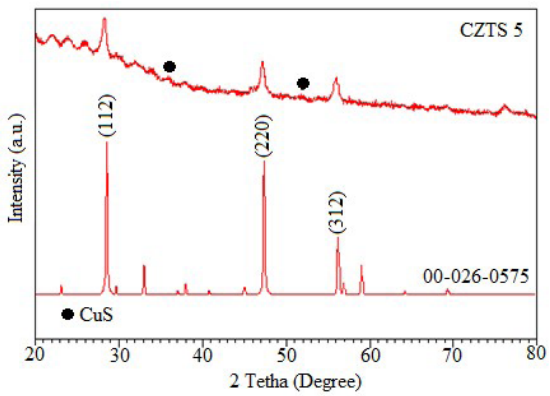

Figure 7. X-ray diffraction pattern for the CZTS5 system calcined under a nitrogen atmosphere at 400°C, showing the absence of the signal associated with the secondary phases.

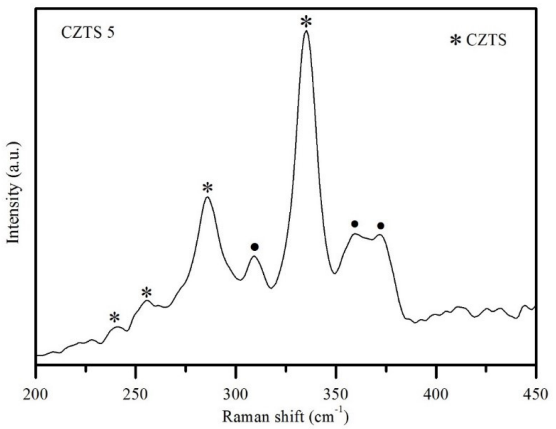

Figure 8. Raman spectrum for the CZTS5 system calcined at 400°C under inert atmosphere conditions.

related to $Cu2_{p3/2}$ and $Cu2_{p1/2}$ are located at 933 and 953 eV respectively, being compatible with an oxidation state 2^+ [55,57]. The $Zn2_{p3/2}$ and $Zn2_{p1/2}$ signals observed at 1023 and 1046 eV were attributed to Zn^{2+} formation. These results agreed with Zhu et al.[58], for the Cu_2ZnSnS_4 system[59]. It should be noted that no satellite peak was observed for Cu^{2+} at 924 eV, which indicates the absence of sulfur or oxide phases in the CZTS5 sample. The C signal at 285 eV suggests incomplete elimination of carbon during the calcination step. Therefore, the observed bindings correspond to the oxidation states of the CZTS materials. However, the carbon and oxygen present in the materials indicate non-homogeneous elemental composition.

3.9. Impedance spectroscopy

The electrical behavior of the CZTS5 material was determined by solid state impedance spectroscopy (IE). The data were taken at room temperature in terms of the real (Z') and an imaginary impedance (Z'_{im}), as shown in Figure 11 in the form of Nyquist graphs.

The graph plotted the complex impedance (Z'_{im}) and the actual impedance (Z'), that revealed a low surface

homogeneity in terms of charge transfer. This behavior is attributed to the nanometer particle sizes or possible defects of the material. The recombination of the grain boundaries hinders the efficient transfer of charge carriers. Particles which are too small and defects potentiate this phenomenon[60,61].

On the other hand, the solid is a semiconductor and presents a conductivity value around 0.00002 $\Omega.cm^{-1}$. Despite the low homogeneity, this value suggests load transfer processes at the electrode-sample interface, so that the electrical microstructure of CZTS5 is consistent with the needs required for solar conversion processes. Additionally, the Bode diagrams, shown in Figure 12, demonstrated regions dominated by capacitive elements, such that the strength of the material decreases with increasing frequency.

This behavior confirms the results obtained from the Nyquist plot and are related to the increase in electrical conductivity. Electrical conductivity values suggest that carrier transport occurs under the concept of thermionic emission (TE) over grain limit barriers[62,63]. The equivalent electric circuit indicates that the material can be modeled with a phase element that is linked to the presence of a certain degree of surface roughness, which would corroborate the development of slow processes in charge transfer, not only in the grain boundaries but also between the electrode-sample interface[57,64]. In addition, a certain degree of poly-crystallinity is suggested in the CZTS5 material, however, it is clear that the conductivity and mobility of the charge carriers improved significantly after the N_2 atmosphere calcination process. Gonzales et al.[65], suggest that the polycrystalline nature is typical for CZTS materials and even the *p*-type conductivity is due to defects in the material, more specifically to CuZn antisites[10,66,67]. Therefore, it is clear that the electrical properties of the CZTS5 material is represented by diffusion and dragging of load carriers and that the intergranular properties determine the transport mechanism and therefore the electrical properties of this material[65]. Indeed, this fact suggests that the CZTS5 solid is a potential candidate to be used as an absorbent layer in thin film technologies, improving the contact conditions.

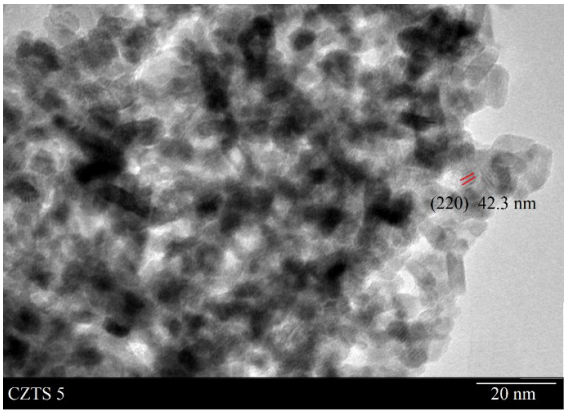

Figure 9. Transmission electron micrograph for the CZTS5 system calcined at 400°C in an inert atmosphere[18].

Figure 13 presents the characteristic curve of the electrical parameters found for the developed photovoltaic cell. In this particular case, the cell exhibits an efficiency of 3.97%, in an area of 0.090 cm^2. The open circuit voltage Voc is located around 1.05 V with a fill factor around 72.7% and a current density of 22.2 mA/cm^2, which confirms a low electrical efficiency in comparison with current results.

However, for CZTS and CZTSe systems it represents an average value, taking into account that in general, the existence of secondary phases, the discontinuity of the layers, mainly of CdS and i-ZnO-ITO could propitiate the formation of cracks over deposited films, which is very difficult to control under deposition conditions, in accordance with reports of Muhunthan et al.[68].

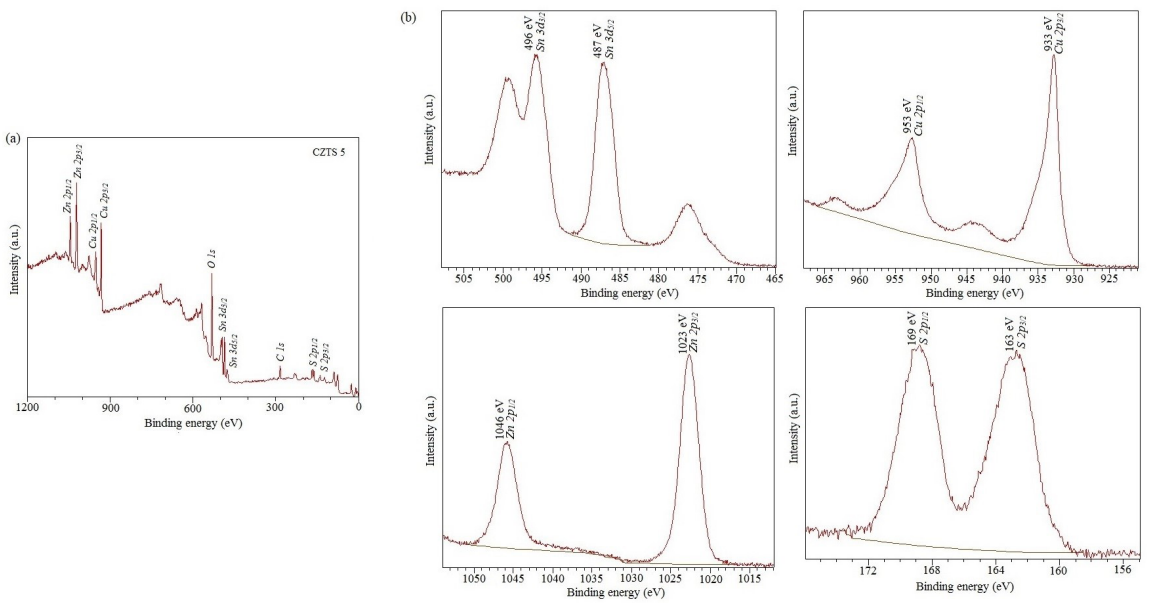

Figure 10. (a) XPS spectra for the CZTS5 material with scanning over the entire energy range. (b)XPS spectra for the CZTS5 material with scanning over the entire energy range with exploration for S*2p*, Sn*3d*, Cu*2p* and Zn*2p*.

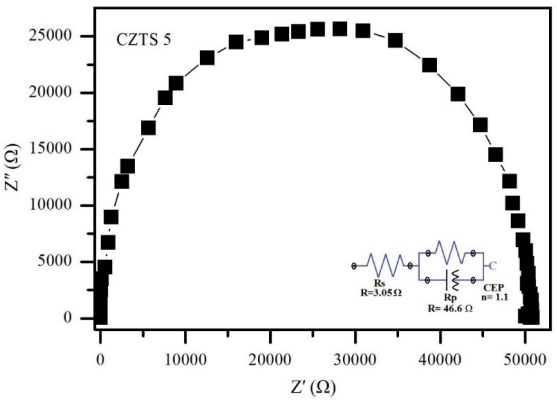

Figure 11. Nyquist diagram for CZTS5.

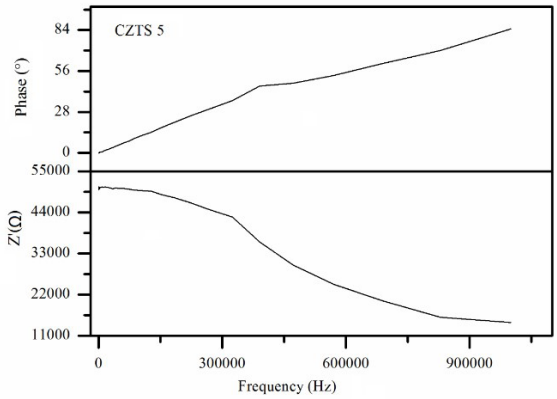

Figure 12. Bode diagrams for the CZTS5 system calcined at 400°C under inert atmosphere.

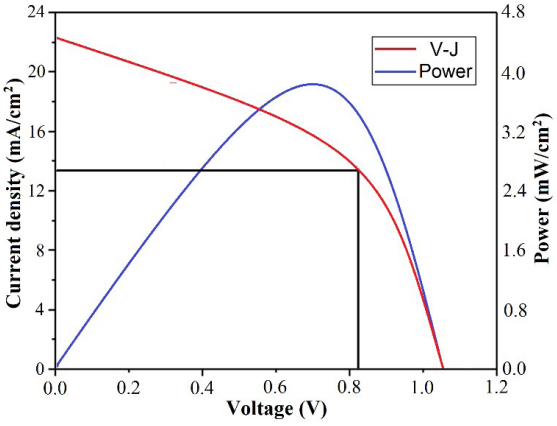

Figure 13. V-I curve and power for the photovoltaic cell assembled with an absorbing layer of CZTS5.

In this way, the developed work for a compound poor in Zn, different from traditional works, but with standard efficiencies, suggests to work with new compositions using the hydrothermal route to promoting the formation of a pure Kesterite phase, improving results.

4. Conclusions

The Cu_2ZnSnS_4 material was obtained successfully using a hydrothermal treatment, and demonstrating the importance of calcination temperature in N_2 atmosphere for the formation of the Kesterite phase, minimizing the formation of secondary phases of Cu. The synthesized material showed a Band-gap around 1.54 eV, nano-sized particles (41.6 nm), preferred crystallographic orientation along the (112) facet and a semiconductor behavior. The XPS results showed the surface chemical composition, allowing estimate the stoichiometry, chemical state and electronic structure of the elements that make up the materials with a good level of correlation, ruling out the presence of contaminants that could have affected the nature of the solids. The electrical behavior of CZTS5 material is attributed to the diffusional processes of loads in grain boundaries, while the conductivity values are in accordance with a semiconductor nature, which suggests that this material CZTS5 is suitable and potentially applicable as an absorbent layer in thin films of CZTS. The final electrochemical characterization, making use of a standard assembly for the validation of the efficiency of the solar cell assembled using the most promising material of CZTS5, showed that the efficiency values obtained are relatively good. Such factors, can be improved and worked in a way much more detailed correcting aspects such as those related to the purity of the crystalline phase, the reduction of the problems associated with the rupture of the layers deposited by means of more specialized techniques than the chemical bath; which caused some difficulties along deposition of i-ZnO and ITO layers, whose heterogeneity could play a crucial role in the efficiency of the device.

5. Acknowledgments

This work was supported by INCITEMA (Instituto para la Investigación e Innovación en Ciencia y Tecnología de Materiales). Universidad Pedagógica y Tecnológica de Colombia. The authors would like to acknowledge the Solid State Chemistry research group of Department of Inorganic and Organic Chemistry of the Universitat Jaume I (UJI), Castellón de la Plana, Spain, for the support in the electrical characterization of the developed solar cell.

6. References

1. International Energy Agency. Global CO_2 emissions in 2019. France: IEA; 2019.
2. National Oceanic Atmospheric Administration. Earth System Research Laboratory. Boulder, CO: Global Monitoring Division. 2020
3. Dang H. Nanostructured semiconductor device design in solar cells [dissertation]. Lexington, Kentucky: Electrical and Computer Engineering, University of Kentucky UKnowledge; 2015.
4. Ruíz A, Krumm A, Schattenhofer L, Burandt T, Montoya F, Oberländer N. Oei Pao-Yu. Solar PV generation in Colombia - A qualitative and quantitative approach to analyze the potential of solar energy market. Renew Energy. 2020;148:1266-79.
5. Perez V, Boix P, Velásquez J, Sorli P, Escaray F, García E, et al. Presente y futuro de las tecnologías verdes: contribuciones desde la Universitat de València. Universitat de València. 2020
6. Mohammed T, Koh S, Reaney I, Acquaye A, Schileo G, Mustapha K, et al. Perovskite solar cells: an integrated hybrid lifecycle assessment and review in comparison with other photovoltaic technologies. Renew Sustain Energy Rev. 2017;80:1321-44.
7. Zhou Z, Wang Y, Xu D, Zhang Y. Fabrication of Cu_2ZnSnS_4 screen printed layers for solar cells. Sol Energy Mater Sol Cells. 2010;94:2042-5.

8. Lu X, Zhuang Z, Peng Q, Li Y. Wurtzite Cu_2ZnSnS_4 nanocrystals: a novel quaternary semiconductor. Chem Commun (Camb). 2011;47:3141-3.
9. Jackson P, Hariskos D, Paetel S. New world record efficiency for Cu(In,Ga)Se_2 thin-film solar cells beyond 20%. Prog Photovolt Res Appl. 2011;19:894-7.
10. Green MA, Emery K, Hishikawa Y, Warta W, Dunlop ED. Solar cell efficiency tables (versión 46). Prog Photovolt Res Appl. 2015;23:805-12.
11. Delbos S. Kësterite thin films for photovoltaics: a review. EPJ Photovolt. 2012;3:35004.
12. Huang W, Tseng C, Chang S, Tuan H, Chiang C, Lyu L, et al. Solvothermal Synthesis of Zinc blende and Wurtzite $CuInS_2$ Nanocrystals and Their Photovoltaic Application. Langmuir. 2012;28:8496-501.
13. Huang S, Luo W, Zou Z. Band positions and photoelectrochemical properties of Cu_2ZnSnS_4 thin films by the ultrasonic spray pyrolysis method. J Phys D Appl Phys. 2013;46:235108-14.
14. Shakban M, Matthews P, Savjani N, Zhong X, Wang Y, Missous M, O'Brien P. The synthesis and characterization of Cu_2ZnSnS_4 thin films from melt reactions using xanthate precursors. J Mater Sci. 2017;52:12761-71.
15. Wang W, Winkler MT, Gunawan O, Gokmen T, Todorov TK, Zhu Y, et al. Device characteristics of CZTSSe thin-film solar cells with 12.6% efficiency. Adv Energy Mater. 2013;45:89.
16. Wang W, Winkler MT, Gunawan O, Gokmen T, Todorov TK, Zhu Y, et al. Device characteristics of CZTSSe thin-film solar cells with 12.6% efficiency. Adv Energy Mater. 2014;4:1301465.
17. Agawane GL, Shin SW, Vanalakar SA, Suryawanshi MP, Moholkar AV, Yun JH, et al. Synthesis of simple, low cost and benign sol–gel Cu_2ZnSnS_4 thin films: influence of different annealing atmospheres. J Mater Sci Mater Electron. 2015;26:1900-7.
18. Sánchez D, Soracá G, Gómez J, Vera E. Synthesis and characterization of the Cu_2ZnSnS_4 system for photovoltaic applications. J. Phys.: Conf. Ser. 2017;786:12-27.
19. Cho J, Ismail A, Park J, Kim W, Yoon S, Min B. Synthesis of Cu_2ZnSnS_4 thin films by a precursor solution paste for thin film solar cell applications. ACS Appl Mater Interfaces. 2013;5:4162-5.
20. Khalate SA, Kate RS, Kim JH, Pawar SM, Deokate RJ. Effect of deposition temperature on the properties of Cu_2ZnSnS_4 (CZTS) thin films. Superlattices Microstruct. 2017;103:335-42.
21. Kannana AG, Manjulavallia TE, Chandrasekaran J. Influence of solvent on the properties of CZTS nanoparticles. Procedia Eng. 2016;141:15-22.
22. Siebentritt S. Why are kesterite solar cells not 20% efficient. Thin Solid Films. 2013;535:1-4.
23. Bao W, Ichimura M. Influence of secondary phases in kesterite-Cu_2ZnSnS_4 absorber material based on the first principles calculation. Int. J. Photo. 2015;2015:1-6.
24. Sun L, He J, Chen Y, Yue F, Yang P, Chu J. Comparative study on Cu_2ZnSnS_4 thin films deposited by sputtering and pulsed laser deposition from a single quaternary sulfide target. J Cryst Growth. 2012;361:147-51.
25. Cheng AJ. Imaging and phase identification of Cu_2ZnSnS_4 thin films using confocal Raman spectroscopy. J Vac Sci Technol A. 2011;29:1-11.
26. Wei M, Du Q, Wang D, Liu W, Jiang G, Zhu C. Synthesis of spindle-like kesterite Cu_2ZnSnS_4 nanoparticles using thiourea as sulfur source. Mater Lett. 2012;79:177-9.
27. Gao Y, Yang H, Zhang Y, Li J, Zhao H, Feng J, et al. Facile non-injection synthesis of high quality CZTS nanocrystals. RSC Advances. 2014;4:17667-70.
28. Gusain M, Kumar P, Uma S, Nagarajan R. Synthesis of Zinc blende $CuInS_2$ and Fe-substituted $CuInS_2$ by the reaction of binary colloids. Colloid Surface A. 2015;481:269-75.
29. Li X, Qian X, Cao YQ, Cao ZY, Liu XJ, Zhu L, et al. A facile and low-cost synthesis of $Cu_2ZnSn(S_xSe_{1-x})_4$ nanocrystals with tunable composition and optical Band-gap. Mater Lett. 2015;150:12-5.
30. He J, Sun L, Chen S, Chen Y, Yang P, Chu J. Composition dependence of structure and optical properties of $Cu_2ZnSn(S,Se)_4$ solid solutions: an experimental study. J Alloys Compd. 2012;511:129-32.
31. Jiang C, Lee JS, Talapin DV. Soluble precursors for $CuInSe_2$, $CuIn_{1-x}Ga_xSe_2$, and $Cu_2ZnSn(S,Se)_4$ Based on Colloidal Nanocrystals and molecular metal chalcogenide surface ligands. J Am Chem Soc. 2012;134:5010-3.
32. Agawane GL, Shin SW, Vanalakar SA, Suryawanshi MP, Moholkar AV, Yun JH, Jihye G, Jin HK, Agawane G. Synthesis of simple, low cost and benign sol–gel Cu_2ZnSnS_4 thin films: Influence of different annealing atmospheres. J Mater Sci Mater Electron. 2015;26:1900-7.
33. Rajesh G, Muthukumarasamy N, Subramaniam EP, Agilan S, Velauthapillai D. Synthesis of Cu_2ZnSnS_4 thin films by dip-coating method without sulphurization. J Sol-Gel Sci Technol. 2013;66:288-92.
34. Hurtado M. Síntesis y caracterización de películas delgadas del semiconductor Cu_2ZnSnS_4 y su uso como capa absorbente en celdas solares [dissertation]. Bogotá (DC): Universidad Nacional de Colombia; 2014.
35. Liu WS, Chen SY, Huang CS, Lee MY, Kuo HC. Investigation of Zn/Sn ratio for improving the material quality of CZTS thin films with the reduction of $Cu_{2-x}S$ secondary phase. J Alloys Compd. 2021;853:157237.
36. Vishwakarma M, Agrawal K, Hadermann J, Mehta BR. Investigating the effect of sulphurization on volatility of compositions in Cu-poor and Sn-rich CZTS thin films. Appl Surf Sci. 2020;507:145043.
37. Tiong V, Zhang Y, Bell J, Wang H. Phase selective Hydrothermal Synthesis of Cu_2ZnSnS_4 Nanocrystals: The effect of the Sulphur Precursor. Cryst Eng Comm. 2014;16:4306-4313.
38. Fairbrother A, García E, Izquierdo V, Fontané X, Agudelo F, Galán O, Rodríguez A, Saucedo E. Development of a selective chemical etch to improve the conversion efficiency of Zn-rich Cu_2ZnSnS_4 solar cells. J Am Chem Soc. 2012;134:8018-21.
39. Agawane GL, Shin SW, Vanalakar SA, Suryawanshi MP, Moholkar AV, Yun JH, et al. Synthesis of simple, low cost and benign sol–gel Cu_2ZnSnS_4 thin films: influence of different annealing atmospheres. J Mater Sci Mater Electron. 2015;26:1900-7.
40. Yin X, Qi G, Gong H. CZTS-based materials and interfaces and their effects on the performance of thin film solar cells. Phys Status Solidi Rapid Res Lett. 2014;08:735-62.
41. Zhou Z, Wang Y, Zhang Y, Xu D. Fabrication of Cu_2ZnSnS_4 screen printed layers for solar cells. Sol Energy Mater Sol Cells. 2010;94:2042-5.
42. Lu X, Zhuang Z, Peng Q, Li Y. Wurtzite Cu_2ZnSnS_4 nanocrystals: A novel quaternary semiconductor. Chem Commun (Camb). 2011;47:3141-3.
43. Wang H, Yasin A, Quitoriano NJ, Demopoulos GP. Aqueous-Based Binary Sulfide Nanoparticle Inks for Cu_2ZnSnS_4 Thin Films Stabilized with Tin(IV). Chalcogenide Complexes. J. Nanomater. 2019;9:1382.
44. Khare A, Himmetoglu B, Johnson M, Norris DJ, Cococcioni M, Aydil ES. Calculation of the lattice dynamics and Raman spectra of copper zinc tin chalcogenides and comparison to experiments. J Appl Phys. 2012;111:083707.
45. Osama A. Synthesis, processing, and fundamental phase formation study of CZTS films for solar cell applications [dissertation]. Miami: Florida International University; 2018.
46. Gürel T, Sevik C, Çağın T. Characterization of vibrational and mechanical properties of quaternary compounds Cu_2ZnSnS_4 and $Cu_2ZnSnSe_4$ in kesterite and stannite structures. Phys Rev B Condens Matter Mater Phys. 2011;84:205-201.

47. Khare A, Himmetoglu B, Cococcioni M, Aydil E. First principles calculation of the electronic properties and lattice dynamics of $Cu_2ZnSn(S_{1-x}\ Se_x)_4$. J Appl Phys. 2012;111:123704.
48. Grossberg M, Krustok J, Raudoja J, Timmo K, Altosaar M, Raadik T. Photoluminescence and Raman study of $Cu_2ZnSn(Se_xS_{1x})_4$ monograins for photovoltaic applications. Thin Solid Films. 2011;519:7403-6.
49. Huang W, Tseng C, Chang S, Tuan H, Chiang C, Lyu L, et al. Solvothermal synthesis of zinc blende and wurtzite $CuInS_2$ nanocrystals and their photovoltaic application. Langmuir. 2012;28:8496-85501.
50. Zhou J, Ye Z, Wang Y, Yi Q, Wen J. Solar Cell Material Cu_2FeSnS_4 Nanoparticles Synthesized Via a facile Liquid Reflux Method. Mater Lett. 2015;140:119-22.
51. Shen J, Zhang D, Li J, Li X, Sun Z, Huang S. Fabrication and evaluation of low-cost $Cu_2ZnSn(S,Se)_4$ counter electrodes for dye-sensitized solar cells. Nano-Micro Lett. 2013;5:281-8.
52. Jitendra K, Sarang I. Evolution of the microstructural, electrical and optical characteristics of sol-gel derived Cu_2ZnSnS_4 thin films during sulfurization. Mater Sci Semicond Process. 2019;91:31-40.
53. Tumbu A, Aslan F, Göktaş A, Mutlu IH. All solution processed superstrate type Cu_2ZnSnS_4 (CZTS) thin film solar cell: effect of absorber layer thickness. J Alloys Compd. 2019;781:280-8.
54. Engberg SL, Schou J, Lam YM. Cu_2ZnSnS_4 nanoparticle absorber layers for thin-film solar cells [dissertation]. Lyngby, Denmark: Technical University of Denmark; 2016.
55. Xu J, Yang X, Yang Q, Wong T, Lee C. Cu_2ZnSnS_4 hierarchical microspheres as an effective counter electrode material for quantum dot sensitized solar cells. J Phys Chem C. 2012;116:19718-23.
56. Lugo JR. Estudio de la velocidad de corrosión en acero estructural astm a-36 con recubrimiento orgánico, empleando espectroscopía de impedancia electroquímica [dissertation]. Cumaná: Universidad de Oriente; 2012.
57. Zhu L, Qiang Y, Zhao Y, Gu X. Double junction photoelectrochemical solar cells based on $Cu_2ZnSnS_4/Cu_2ZnSnSe_4$ thin films as composite photocathode. Appl Surf Sci. 2014;292:55-62.
58. Cui Y, Wang G, Pan D. Colloidal synthesis and optical properties of metastable wurtzite I_3-III-IV-VI_5 (Cu_3InSnS_5) nanocrystals. CrystEngComm. 2013;15:10459-63.
59. Tao H, Cao F, Zhang C, Chen S, Tan B, Tao J. In-situ growth of Cu_2ZnSnS_4 nanoparticles on thiol reduce graphene oxide for Cu_2ZnSnS_4-sensitized solar cells. J Alloys Compd. 2017;698:114-20.
60. Kumar M, Dubey A, Adhikari N, Venkatesan S, Qiao Q. Strategic review of secondary phases, defects and defect-complexes in kesterite CZTS–Se solar cells. Energy Environ Sci. 2015;8:3134-59.
61. Guo BL, Chen YH, Liu XJ, Liu WC, Li AD. Optical and electrical properties study of sol-gel derived Cu_2ZnSnS_4 thin films for solar cells. AIP Adv. 2014;4:097115-24.
62. Ghediya P, Chaudhuri T, Ray J. Effect of light on hopping conduction in Kesterite CZTS Thin Films. AIP Conf Proc. 2015;1728:020020-1-020020-4.
63. Elizabeth VH. Impedance Spectroscopy for Emerging Photovoltaics. J Phys Chem C. 2019;123:11329-46.
64. Gonzalez J, Ribeiro G, Viana E, Fernandes P, Salome P, Gutierrez K, et al. Hopping conduction and persistent photoconductivity in Cu_2ZnSnS_4 thin films. J Phys D Appl Phys. 2013;46:155107-13.
65. Fernandes PA, Salome PMP, Da Cunha AF. A study of ternary Cu_2SnS_3 and Cu_3SnS_4 thin films prepared by sulfurizing stacked metal precursors. J Phys D Appl Phys. 2010;43:215403-13.
66. Chen S, Yang J, Gong X, Walsh A, Wei S. Intrinsic point defects and complexes in the quaternary kesterite semiconductor Cu_2ZnSnS_4. Phys Rev B Condens Matter Mater Phys. 2010;81:204-45.
67. Muhunthan N, PalSingh O, Toutam V, Singh VN. Electrical characterization of grain boundaries of CZTS thin films using conductive atomic force microscopy techniques. Mater Res Bull. 2015;70:373-8.
68. Xavier F. Caracterización por espectroscopía Raman de semiconductores Cu_2ZnSnS_4 para nuevas tecnologías fotovoltáicas [dissertation]. España: Universidad de Barcelona; 2013.

Supplementary material

The following online material is available for this article:
Figure S1 - Hydrothermal synthesis of the CZTS materials (CZTS 1- CZTS 5)